

Preparation of Three-Dimensional Graphene and Myoglobin Modified Electrode for Electrocatalysis of Trichloroacetic Acid

Hui Xie¹, Juan Liu², Zuorui Wen¹, Guiling Luo¹, Yanyan Niu¹, Xiaobao Li¹, Guangjiu Li², Wei Sun^{1,*}

¹ Key Laboratory of Water Pollution Treatment and Resource Reuse of Hainan Province, Key Laboratory of Functional Materials and Photoelectrochemistry of Haikou, College of Chemistry and Chemical Engineering, Hainan Normal University, Haikou 571158, P R China

² Key Laboratory of Optic-electric Sensing and Analytical Chemistry for Life Science of Ministry of Education, College of Chemistry and Molecular Engineering, Qingdao University of Science and Technology, Qingdao 266042, P R China

*E-mail: swyy26@hotmail.com

Key Laboratory of Water Pollution Treatment and Resource Reuse of Hainan Province

Received: 16 March 2019 / Accepted: 21 May 2019 / Published: 30 June 2019

In this paper three-dimensional graphene (3DGR) was synthesized by hydrothermal method and further used as electrode modifier on the surface of carbon ionic liquid electrode (CILE). Then an electrochemical biosensor was prepared by further immobilizing myoglobin (Mb) and chitosan (CTS) on the electrode surface in sequence. Spectral results showed that Mb immobilized with 3DGR maintained its original structure. Cyclic voltammogram of CTS/Mb/3DGR/CILE in pH 4.0 phosphate buffer solution gave a pair of quasi-reversible redox peak, indicating that direct electrochemistry of Mb had been achieved on the electrode, which was attributed to the specific macrostructure of 3DGR with high conductivity and large interconnected network. By using CTS/Mb/3DGR/CILE as the working electrode, a third-generation electrochemical biosensor was constructed for the detection of trichloroacetic acid with the linear range from 16.0 to 80.0 mmol/L and the detection limits calculated as 5.33 mmol/L. Experimental results extended the application of 3DGR in the electrode modification with advantages such as high sensitivity, wide detection range, good stability and reproducibility.

Keywords: carbon ionic liquid electrode, three-dimensional graphene, myoglobin, electrochemistry, trichloroacetic acid

1. INTRODUCTION

Redox proteins are biomolecules that are responsible for many important functions in organisms, which can be used to devise different bioelectronic equipments [1-3]. Due to the surrounding of active site of the redox proteins by intricate polypeptide chains, the electron transfer

process is difficult to realize [4]. Therefore, it is necessary to construct a conductive interface for rapid electron exchange between proteins and electrodes.

Two-dimensional graphene (2DGR) is a planar nanosheet that formed by carbon atoms sp^2 hybridization, which has the advantages such as larger specific surface area, higher electron transfer rate, and better flexibility [5]. Therefore GR and its related composites have been synthesized and used in the fields of electrochemical applications [6-10]. Also 2DGR can be assembled into three-dimensional graphene (3DGR) macrostructure, which not only inherits excellent physical and chemical properties of 2DGR, but also processes many unique properties including cross-linked pore structure, high thermodynamic and chemical stability [11,12]. Various preparation methods of 3DGR including self-assembly [13], chemical vapor deposition [14] and template-mediated synthesis [15] have been devised. For example, Shi et al. prepared 3DGR by hydrothermal self-assembly using an aqueous solution of graphene oxide [16]. Chen et al. deposited CH_4 onto a 3D foamed nickel skeleton by chemical vapor deposition at high temperature and pressure to get a 3DGR film with large specific surface area [17]. Schaedler et al. fabricated a 3DGR by using a template method with the density of 1.2 mg/cm^3 [18].

In this paper, 3DGR was synthesized by one-step hydrothermal method, which was immobilized on the surface of carbon ionic liquid electrode (CILE) to obtain 3DGR/CILE. CILE is an ionic liquid modified carbon paste electrode with excellent electrochemical performances, which has been extensively used as the basic working electrodes for electroanalysis [19-23]. Then myoglobin (Mb) molecule and chitosan (CTS) were further drop-casted onto the surface of 3DGR/CILE to obtain CTS/Mb/3DGR/CILE. The porous structure of 3DGR can provide more attachment site for Mb with good biocompatibility, specific electron transfer capability and large effective surface area, which is benefit for the realization of electron transfer of Mb with electrode. Direct electron transfer of Mb on 3DGR modified electrode was achieved and electrocatalytic performance to the reduction of trichloroacetic acid (TCA) was tested by CTS/Mb/3DGR/CILE.

2. EXPERIMENTAL

2.1 Instruments

CHI 1210A and CHI 750B electrochemical workstations (Shanghai Chenhua Instrument Co., China) were used with a three-electrode system including self-made CTS/Mb/3DGR/CILE as working electrode, saturated calomel electrode (SCE) as reference electrode, platinum plate as auxiliary electrode. Nicolet 6700 Fourier transform infrared spectrometer (Thermo Scientific, USA), TU-1901 dual-beam UV-visible spectrophotometer (Beijing Pu's General Instrument Co., Ltd., China) and JSM-7100F scanning electron microscope (SEM, Japan Electronics Corporation, Japan) were used for characterization.

2.2 Reagents

N-hexylpyridinium hexafluorophosphate (HPPF₆, Lanzhou Yulu Fine Chem. Co., China), graphene oxide (GO, Shanxi Tanmei Technology Co., China), graphite powder (Shanghai Colloid

Chem. Co., China), myoglobin (Mb, MW. 17800, Sigma, USA), TCA (Tianjin Komio Reagent Chem. Co., China) and chitosan (CTS, Dalin Xindie Chem. Co., China) were used as received. Phosphate buffer solution (PBS, 0.1 mol/L) was prepared as the supporting electrolyte and doubly distilled water was used throughout this study. The reagents used were of analytical grade, and the buffer solution was filled by nitrogen for 30 min before experiment with electrochemical experiments carried out under N₂ atmosphere.

2.3 Synthesis of 3DGR

3DGR was synthesized by a one-step hydrothermal method with the following procedure. 20 mL of 2.0 mg/mL GO aqueous solution was ultrasonicated for 1 hour, transferred to a 50 mL teflon lined stainless-steel autoclave, heated at 180 °C for 12 h, and cooled at room temperature to obtain a cylindrical 3DGR hydrogel. After washing three times with ethanol and lyophilizing at -87 °C for 12 h, 3DGR were obtained.

2.4 Preparation of Mb modified electrode

According to previous report [24], CILE was hand-made by mixing HPPF₆ and graphite powder with a glass electrode tube ($\Phi=4$ mm), which was polished on a piece of polishing paper just before use.

8.0 μ L of 0.8 mg/mL 3DGR dispersion was dropcasted on the surface of CILE and dried to form a 3DGR/CILE. Then 8.0 μ L of 15.0 mg/mL Mb solution was immobilized on the surface of 3DGR/CILE and dried to obtain Mb/3DGR/CILE. Finally, a CTS (1.0% HAC) solution was applied on Mb/3DGR/CILE and dried naturally to obtain CTS/Mb/3DGR/CILE.

3. RESULTS AND DISCUSSION

3.1 Study on the morphology of 3DGR

The photo of 3DGR hydrogel and scanning electron microscopic results were displayed in Fig.1. The GO aqueous solution appeared as homogeneously dark-brown (Fig.1A) and a cylindrical 3DGR hydrogel was obtained after the hydrothermal reaction, indicating the successfully reduction of GO (Fig.1B). The results can be attributed to the oxygen-containing groups of GO are continuously removed and the conjugated groups are continuously restored and repaired, so that electrostatic repulsion between GO sheets are reduced and the π - π interaction is enhanced. The SEM images of 3DGR under different magnifications was shown in Fig.1C and D, which gave large pore sizes with a spatial 3D structure that compared with 2DGR nanosheet. The 3D structure indicated that the specific surface area is much larger than that of 2DGR, which help more protein/enzyme to adhere on and inside the surface. In addition, the porous channel structure can also provide a faster and smoother way for ion diffusion and electron transfer.

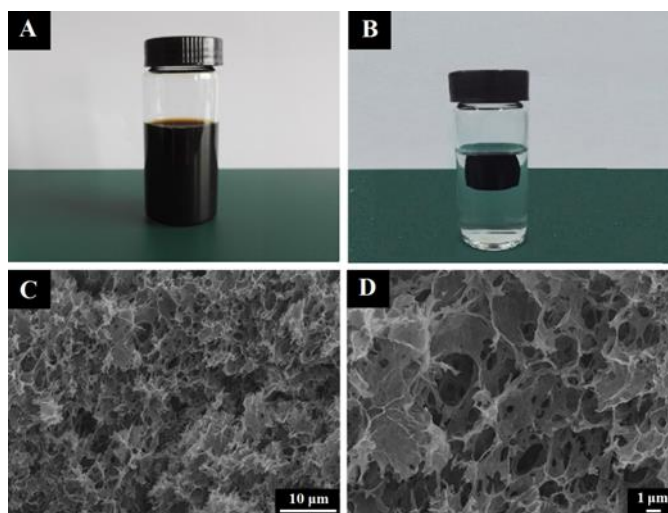


Figure 1. Photo of (A) GO solution, (B) 3DGR hydrogel and scanning electron micrograph of 3DGR at different magnifications (C and D).

3.2 Spectral results

UV-Vis absorption spectrum can be utilized to check whether the structure of protein's denatured. If the active sites in the protein are destroyed or inactivated, the Soret band of the ferric iron in the spectrum will migrate or disappear [25]. As shown in Fig.2A, the Soret absorption band of Mb molecule was located at 436.0 nm (curve a). When Mb was blended with 3DGR, the Soret absorption band (curve b) kept unchanged, which indicated that the active site remained after Mb mixed with 3DGR.

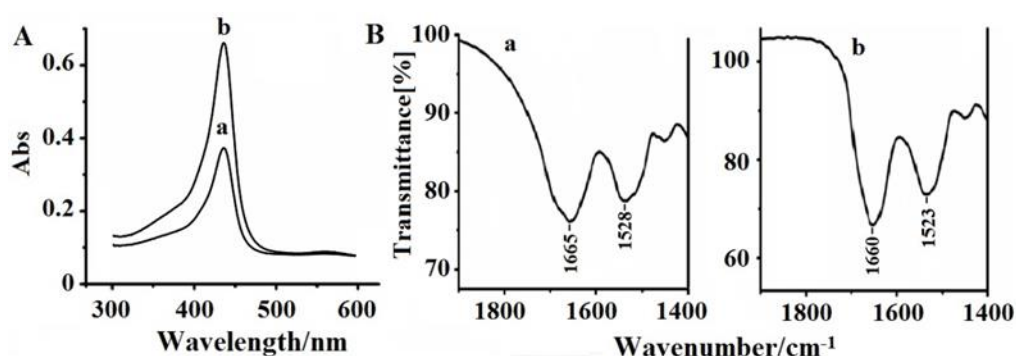


Figure 2. (A) UV-Vis absorption spectra (a) Mb and (b) Mb-3DGR mixture; (B) FT-IR spectra (a) Mb and (b) Mb-3DGR mixture.

Fourier transform infrared spectroscopy (FT-IR) can also be used to identify secondary structures of protein by observing the position and shape of the amide I ($1700\text{--}1600\text{ cm}^{-1}$) and the amide II ($1620\text{--}1500\text{ cm}^{-1}$) band in the spectrum [26]. As shown in Fig.2B, the absorption bands of amide I and amide II of Mb were located at 1665 cm^{-1} and 1528 cm^{-1} (curve a). When Mb was mixed with 3DGR, the absorption bands were located at 1660 cm^{-1} and 1523 cm^{-1} (curve b). It can be

concluded that these two peaks were basically coincident and Mb was not denatured after mixed with 3DGR. All the spectroscopic results indicated that Mb still remained its structure after mixed with 3DGR due to its good biocompatibility.

3.3 Electrochemical investigations

EIS is an effective tool to get information about the impedance changes, which can be obtained from the diameter of the semi-circle of the impedance curve. EIS test was carried out in a 0.1 mol/L KCl and 10.0 mmol/L $[\text{Fe}(\text{CN})_6]^{3-/4-}$ solution with the curves shown in Fig.3A. The resistance (Ret) of CTS/CILE (curve c) was 44.5 Ω , and CTS/3DGR/CILE (curve a) had the Ret value as 22.5 Ω , which indicated that the presence of highly conductive 3DGR decreased the surface resistance and accelerated the electron transfer process. The Ret of CTS/Mb/CILE (curve d) increased to 69.2 Ω , indicated that the presence of nonconductive Mb on the electrode hindered electron transfer. The Ret of CTS/Mb/3DGR/CILE (curve b) was reduced significantly to 36.4 Ω , indicated that the positive effect of 3DGR to accelerate the electron transfer with the decrease of interfacial resistance.

Cyclic voltammetric curves of different modified electrodes were also recorded with curves depicted in Fig.3B. On CTS/3DGR/CILE (curve a) the redox peak current reached a maximum, which was ascribed to the high conductive 3DGR on the surface of CILE increased the electrochemical response. While the redox peak currents decreased gradually on CTS/Mb/3DGR/CILE (curve b), CTS/CILE (curve c) and CTS/Mb/CILE (curve d), which proved that the presence of nonconductive Mb on the CILE was not benefit for the electrochemical reaction of $[\text{Fe}(\text{CN})_6]^{3-/4-}$.

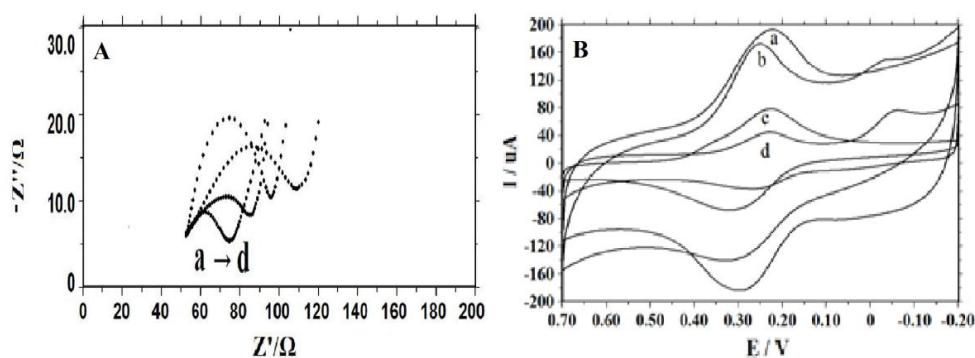


Figure 3. (A) EIS results of different modified electrodes, (a) CTS/3DGR/CILE, (b) CTS/Mb/3DGR/CILE, (c) CTS/CILE and (d) CTS/Mb/CILE in a 10.0 mmol/L $[\text{Fe}(\text{CN})_6]^{3-/4-}$ and 0.1 mol/L KCl solution; (B) Cyclic voltammetric curves of different modified electrodes (a) CTS/3DGR/CILE, (b) CTS/Mb/3DGR/CILE, (c) CTS/CILE and (d) CTS/Mb/CILE in a 1.0 mmol/L $[\text{Fe}(\text{CN})_6]^{3-/4-}$ and 0.5 mol/L KCl solution with the scan rate of 0.1 V/s.

3.4 Direct electrochemistry of CTS/Mb/3DGR/CILE

Cyclic voltammograms of different modified electrodes in 0.1 mol/L PBS (pH 4.0) with the scan rate of 0.1 V/s were shown in Fig.4. No redox peaks were observed on CTS/3DGR/CILE (curve

c), CTS/CILE (curve d) and CILE (curve e), indicating that no redox reaction occurred in the selected potential window for three electrodes. However, due to the presence of 3DGR, the surface area of the electrode was increased and formed an interfacial electric double layer, which significantly increased the background current of curve c. The redox peak appeared on CTS/Mb/3DGR/CILE (curve a) and CTS/Mb/CILE (curve b) with Mb present on the electrode, indicating that redox reaction appeared with electron transfer of Mb realized. CILE has been reported to be a high-efficiency electrode [27], which can facilitate the direct electron transfer of redox protein on CILE. While on CTS/Mb/3DGR/CILE (curve a) the redox current signals magnified, which was ascribed to the presence of high conductive 3DGR with porous structure that improved the loading capacity of Mb molecule and facilitated the electron transfer. The formal peak potential (E^0) was calculated as -0.285 V (vs. SCE), which was close to the reported values such as -0.295 V for the Ag-doped CNTs modified electrode [28] and -0.304 V for the DNA-modified electrode [29].

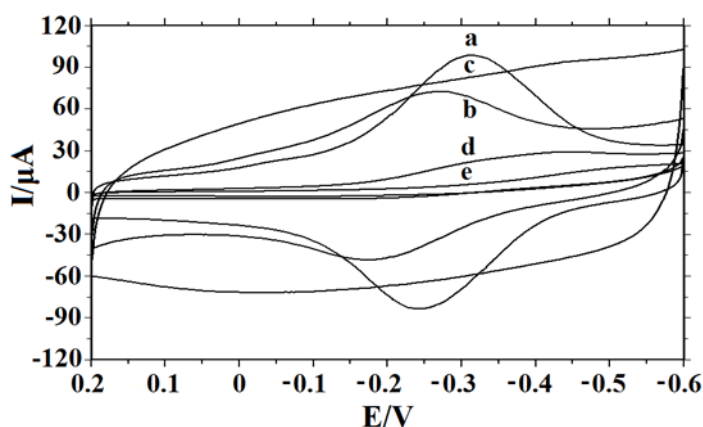


Figure 4. Cyclic voltammograms of (a) CTS/Mb/3DGR/CILE, (b) CTS/Mb/CILE, (c) CTS/3DGR/CILE, (d) CTS/CILE and (e) CILE in pH 4.0 PBS with the scan rate as 0.1 V/s.

3.5 Effect of scan rate

Effect of scan rate on CTS/Mb/3DGR/CILE was investigated. As shown in Fig.5A, a pair of symmetric redox peak appeared and the redox peak currents increased gradually with scan rate. In Fig.5B, it can be found that in the range of 50-900 mV/s, both cathodic and anodic peak currents shifted gradually towards opposite directions. The linear regression equations were calculated as I_{pc} (μA) = 324.28 v (V/s) + 2.30 ($n = 10$, $\gamma = 0.999$) and I_{pa} (μA) = -136.63 v (V/s) - 1.65 ($n = 10$, $\gamma = 0.998$). The results showed that Mb on the electrode underwent a classical surface-controlled electrochemical process. In Fig.5C, the anodic and cathodic peak potentials with $\ln v$ exhibited a linear relationship and the regression equations were E_{pc} (V) = -0.040 $\ln v$ - 0.409 ($n = 8$, $\gamma = 0.998$) and E_{pa} (V) = 0.029 $\ln v$ - 0.188 ($n = 8$, $\gamma = 0.998$). According to the following Laviron's equations [30],

$$E_{pa} = E^0 + \frac{RT}{(1-\alpha)nF} \ln v \quad (1)$$

$$E_{pc} = E^{0'} - \frac{RT}{\alpha nF} \ln \nu \quad (2)$$

$$\log k_s = \alpha \log(1-\alpha) + (1-\alpha) \log \alpha - \log \frac{RT}{nF\nu} - \frac{(1-\alpha)\alpha nF \Delta E_p}{2.3RT} \quad (3)$$

The electrochemical parameters including the electron transferred number (n), electron transfer coefficient (α) and the apparent heterogeneous electron transfer rate constant (k_s) were calculated as 1.1, 0.425 and 1.83 s^{-1} , respectively. Since the value of k_s can reflect the microenvironment of Mb, which indicated a typical surface-controlled process of Mb electrochemistry. Compared with other Mb electrodes such as 0.39 s^{-1} [31], 0.41 s^{-1} [32] and 0.584 s^{-1} [33], the k_s value was larger in this paper. It was further indicated that the large specific surface area of 3DGR provided more attachment sites for Mb to transfer electrons more easily. Furthermore, the apparent surface concentration (Γ^*) of Mb was calculated according to Faraday's equation: $Q=nAF\Gamma^*$ [34] with the value as $4.56 \times 10^{-9} \text{ mol/cm}^2$. Therefore it can be confirmed that the presence of 3DGR caused multi-layer of Mb to participate in the electrode reaction.

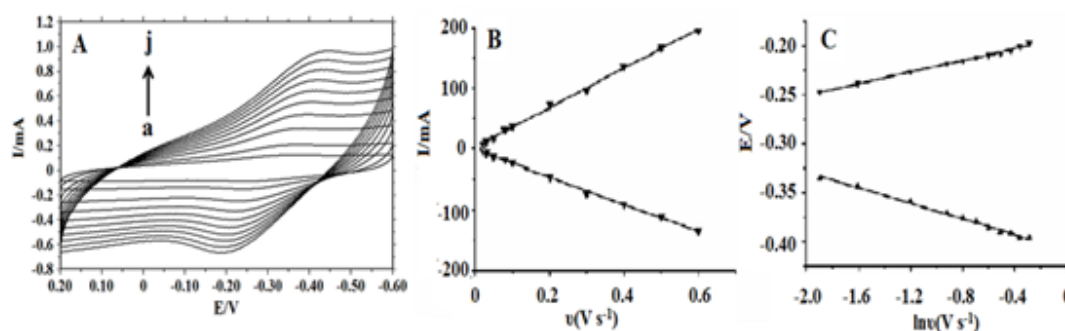
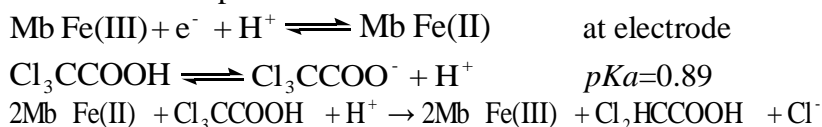


Figure 5. (A) Cycle voltammograms of CTS/Mb/3DGR/CILE at different scan rates (from a to j as 50, 80, 100, 200, 300, 400, 500, 600, 800, 900 mV/s); (B) Linear relationship of the redox peak currents and scan rate (ν); (C) Linear relationship of the redox peak potentials and $\ln \nu$.

3.6 Electrocatalytic behavior of Mb

The electrocatalytic performance of CTS/Mb/3DGR/CILE for TCA was shown in Fig.6, it was observed that the cathodic response increased gradually at -0.326 V while the anodic response was decreased and even disappeared. According to the literature [35], the mechanisms of the catalytic reduction reaction were presented as follows:



Reduction peak current had a good linear equation with TCA concentration from 16.0 to 80.0 mmol/L. The linear regression equation was $I_{ss} (\mu\text{A}) = 3.61 C (\text{mmol/L}) + 8.69$ ($n = 17$, $\gamma = 0.999$)

with the detection limit as 5.33 mmol/L. When the TCA concentration was more than 80.0 mmol·L⁻¹, the responses almost remained steady, shown a Michaelis-Menten dynamic mechanism. The apparent Michaelis-Menten constant (K_M^{app}) was an important indicator for investigating the enzyme-substrate reaction kinetics in an enzyme-catalyzed reaction. According to the Lineweaver-Burk equation: $1/I_{ss} = (1/I_{max}) (1 + K_M^{app}/C)$ [36], the K_M^{app} of the catalytic reaction was calculated as 31.7 mmol/L, indicating better affinity of Mb to the substrate TCA.

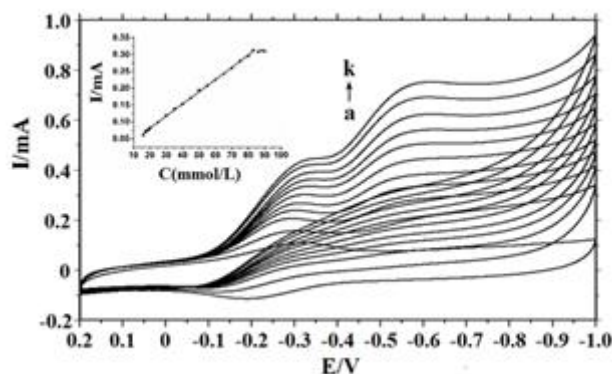


Figure 6. Cyclic voltammograms of CTS/Mb/3DGR/CILE with different concentrations of TCA (from a to k as 0.0, 16.0, 20.0, 25.0, 30.0, 35.0, 40.0, 50.0, 60.0, 70.0, 80.0 mmol/L); inset is the linear relationship of TCA concentration and cathodic current).

3.7 Detection of real sample

The application of CTS/Mb/3DGR/CILE to sample detection was demonstrated in medical facial peel solution (got from Shanghai IKA Biotech. Co., China) with the recovery calculated by standard addition method. As shown in Table 1, the recoveries were in the range of 99.87% to 101.70% with the RSD values from 0.45% to 1.36%. Thus the described sensor can be used for the determination of TCA content in real sample.

Table 1. Analytical data of TCA concentration in real sample by modified electrode (n=3)

Sample	Marked (mmol/L)	Detected (mmol/L)	Added (mmol/L)	Total (mmol/L)	Recovery (%)	RSD (%)
35% Medical facial peel solution	27.17	27.12	10.00	37.29	101.70	1.36
			20.00	47.16	100.20	0.89
			30.00	57.08	99.87	0.45

3.8 Stability and reproducibility of CTS/Mb/3DGR/CILE

The stability was obtained by cyclic voltammetric scan and the current was almost unchanged after continuous scanning for 300 cycles, indicating that Mb was stable in the membrane without loss of biological activity. The prepared CTS/Mb/3DGR/CILE was stored at 4 °C refrigerator for 10 days and the current responses maintained 95.36% of its initial value. After 30 days, the peak current was still as high as 91.47%. The good stability can be attributed to the unique porous structure, good biocompatibility and more active sites, which provided a favorable microenvironment for Mb. Ten electrodes were prepared by the same procedure to detect 20.0 mmol/L TCA and gave a RSD value as 4.19%, which indicated the modified electrode had good reproducibility.

4. CONCLUSIONS

In this paper 3DGR with a porous structure was synthesized by one-step hydrothermal method, which was used for effectively immobilization of Mb. Also 3DGR had a large specific surface area, which enabled multi-layer of Mb to participate in direct electrochemical reaction. Spectral results showed that the Mb immobilized on 3DGR maintained the original structure. Cyclic voltammetric curve of CTS/Mb/3DGR/CILE in pH 4.0 buffer solution showed a quasi-reversible redox peak, indicating that the direct electrochemistry of Mb was achieved on the electrode and the results extended the application of 3DGR in protein electrochemistry.

ACKNOWLEDGMENTS

This work was supported by the financial support of the National Natural Science Foundation of Hainan Province of China (2017CXTD007), the Key Science and Technology Program of Haikou City (2017042) and Graduate Student Innovation Research Project of Hainan Province (Hys2018-212).

References

1. F.A. Armstrong, H.A.O. Hill and N. J. Walton, *Accounts Chem. Res.*, 21 (1988) 407-413.
2. F.A. Armstrong and G.S. Wilson, *Electrochim. Acta*, 45 (2000) 2623-2645.
3. P. Bianco, *J. Biotechnol.*, 82 (2002) 393-409.
4. J.J. Gooding, R. Wibowo, J. Liu, W. Yang, D. Losic, S. Orbons, F.J. Mearns, J.G. Shapter and D.B. Hibbert, *J. Am. Chem. Soc.*, 125 (2003) 9006-9007.
5. Y.X. Liu, X.C. Dong and P. Chen, *Chem. Soc. Rev.*, 41 (2012) 2283-2307.
6. K.Q. Deng, X.F. Li and H.W. Huang, *Electrochim. Acta*, 204 (2016) 84-91.
7. K.Q. Deng, J.H. Zhou and X.F. Li, *Electrochim. Acta*, 95 (2013) 18-23.
8. K.Q. Deng, J.H. Zhou, H.W. Huang, Y.L. Ling and C.X. Li, *Anal. Lett.*, 49 (2016) 2917-2930.
9. K.Q. Deng, C.X. Li, X.Y. Qiu, J.H. Zhou and Z.H. Hou, *Electrochim. Acta*, 174 (2015) 1096-1103.
10. K.Q. Deng, C.X. Li, H.W. Huang and X.F. Li, *Sensor. Actuat. B-Chem.*, 238 (2017) 1302-1308.
11. C. Li and G. Shi, *Nanoscale*, 4 (2012) 5549-5563.
12. J. Zhu, X. Yang, Z. Fu, J. He, C. Wang, W. Wu and L. Zhang, *Chemistry*, 22 (2016) 2515-2524.
13. Q. Fang, X. Zhou, W. Deng and Z. Liu, *Nanoscale*, 8 (2016) 197-203.
14. L. Zhu, X. Guo, Y. Liu, Z. Chen, W. Zhang, K. Yin, L. Li, Y. Zhang, Z. Wang, L. Sun and Y. Zhao,

Nanotechnology, 2018.

15. X. Yang, A. Liu, Y. Zhao, H. Lu, Y. Zhang, W. Wei, Y. Li and S. Liu, *ACS Appl. Mater. Inter.*, 7 (2015) 23731-23740.
16. Y. Xu, K. Sheng, C. Li and G. Shi, *ACS Nano*, 4 (2010) 4324.
17. Z.P. Chen, W.C. Ren and L.B. Gao, B. Liu, S. Pei and H.M. Cheng, *Nat. Mater.*, 10 (2011) 424-428.
18. T.A. Schaedler, A.J. Jacobsen, A. Torrents, A.E. Sorensen, J. Lian, J.R. Greer, L. Valdevit and W.B. Carter, *Science*, 334 (2011) 962-965.
19. X.L. Niu, W. Chen, X.L. Wang, Y.L. Men, Q. Wang, W. Sun and G.J. Li, *Microchim. Acta*, 185 (2018) 167.
20. Y.Y. Niu, J. Liu, W. Chen, C.X. Yin, W.J. Weng, X.Y. Li, X.L. Wang, G.J. Li and W. Sun, *Anal. Methods-UK*, 10 (2018) 5297-9504.
21. W. Chen, W.J. Weng, X.L. Niu, X.Y. Li, Y.L. Men, W. Sun, G.J. Li and L.F. Dong, *J. Electroanal. Chem.*, 823 (2018) 137-145.
22. G.L. Luo, H. Xie, Y.Y. Niu, J. Liu, Y.Q. Huang, B.H. Li, G.J. Li and W. Sun, *Int. J. Electrochem. Sci.*, 14 (2019) 2405-2413.
23. J. Liu, W.J. Weng, C.X. Yin, G.L. Luo, H. Xie, Y.Y. Niu, X.Y. Li, G.J. Li, Y.R. Xi, Y.T. Gong, S.Y. Zhang and W. Sun, *Int. J. Electrochem. Sci.*, 14 (2019) 1310-1317.
24. R.Y. Zou, X.B. Li, G.L. Luo, Y.Y. Niu, W.J. Weng, W. Sun, J.W. Xi, Y. Chen and G.J. Li, *Electroanal.*, 31 (2019) 575-581.
25. J.F. Rusling and A.F. Nassar, *J. Am. Chem. Soc.*, 115 (1993) 11891-11897.
26. A.E.F. Nassar, J.M. Bobbitt and J.D. Stuart, *J. Am. Chem. Soc.*, 117 (1995) 729-735.
27. W. Sun, D.D. Wang, R.F. Gao and K. Jiao, *Electrochem. Commun.*, 9 (2007) 1159-1164.
28. C.Y. Liu and J.M. Hu, *Biosens. Bioelectron.*, 24 (2009) 2149-2154.
29. R.F. Gao and J.B. Zheng, *Electrochem. Commun.*, 11 (2009) 1527-1529.
30. E. Laviron, *J. Electroanal. Chem.*, 101 (1979) 19-28.
31. Q.L. Wang, G.X. Lu and B.J. Yang, *Langmuir*, 20 (2004) 1342-1347.
32. A.B. Moghaddam, M.R. Ganjali, R. Dinarvand, S. Ahadi and A.A. Saboury, *Biophys. Chem.*, 134 (2008) 25-33.
33. W. Sun, L.F. Li, B.X. Lei, T.T. Li, X.M. Ju, X.Z. Wang, G.J. Li and Z.F. Sun, *Mat. Sci. Eng. C-Mater.*, 33 (2013) 1907-1913.
34. A.J. Bard and L.R. Faulkner, Wiley, New York, 1980.
35. C.H. Fan, G.X. Li, J.Q. Zhu, D.X. Zhu, *Anal. Chim. Acta*, 423 (2000) 95-100.
36. R.A. Kamin and G.S. Wilson, *Anal. Chem.*, 52 (1980) 1198-1205.

© 2019 The Authors. Published by ESG (www.electrochemsci.org). This article is an open access article distributed under the terms and conditions of the Creative Commons Attribution license (<http://creativecommons.org/licenses/by/4.0/>).